Wavelet Image Interpolation (WII):A Wavelet-based Approach to Enhancement of Digital Mammography Images

G. Derado[1], F.D. Bowman[1], R. Patel[1,2], M. Newell[3], B. Vidakovic[1,4]

[1] Department of Biostatistics, Emory University, Atlanta, GA
[2] Amgen Inc., Thousand Oaks, CA
[3] Department of Radiology, Emory University, Atlanta, GA
[4] Georgia Institute of Technology, Atlanta, GA

Abstract. Cancer detection using mammography focuses, in part, on characteristics of tiny microcalcifications, including the number, size, and spatial arrangement of the microcalcifications, as well as morphological features of individual microcalcifications. We have developed state-of-the-art wavelet-based methods to enhance the resolution of microcalcifications visible on digital mammograms, aimed at improving the specificity of breast cancer diagnoses. In our research, we develop, refine, and evaluate a Wavelet Image Interpolation (WII) procedure and create accompanying software to implement it. WII involves the application of an inverse wavelet transformation to a coarse or degraded image and constructed detail coefficients to produce an enhanced higher resolution image. The construction of detail coefficients is supervised by the observed image and innate regular scaling assessed by a statistical model. We found that our proposed procedure is efficient and useful in capturing relevant clinical information in the context of digital mammographic imaging. Our proposed methodology was tested by an experienced radiologist in a study using 40 images from the University of South Florida Digital Database for Screening Mammography (DDSM).

1 Introduction

In the United States, breast cancer is the second leading cause of death in women. One out of eight women will develop breast cancer in her lifetime. Studies have indicated that early detection and treatment improve the chances of survival for breast cancer patients (Curpen *et al.* [6], Smart *et al.* [20]). At present, mammography is the only proven method that can reduce breast cancer mortality through early detection. Attempts to increase the specificity of mammmographic diagnoses, and therefore to reduce the number of unnecessary biopsies, are based on the evaluation of the number , size, and spatial arrangement of microcalcifications (Millis *et al.* [18]) as well as morphological features of single microcalcifications (Egan *et al.* [8]). We propose the development and application of novel wavelet-based methods for improving cancer diagnoses by enhancing key features of microcalcifications in digital mammography.

Although there are several findings on a mammogram image that are critical for a cancer diagnosis (masses, architectural distortions, asymmetry), our research focuses on microcalcifications. About half of the cancers detected by mammography appear as a cluster of microcalcifications. Microcalcifications are the most common mammographic sign of ductal carcinoma in situ (DCIS), which is an early stage cancer confined to the breast ducts. Almost 90% of DCIS cases are associated with microcalcifications.

In addition to specific arrangement or distribution, the irregularity of microcalcification shapes is an important attribute. "Pleomorphic" or "heterogeneous" are synonyms for an irregular shape or variability of shapes which can indicate DCIS. Such microcalcifications are usually more conspicuous than the amorphous forms (Coakley and van Doorn [5]). Another malignant form includes fine, linear or fine, linear, branching calcifications. These are thin, irregular calcifications that appear linear, but are discontinuous and under 0.5 mm in width. Their appearance suggests filling of the lumen of a duct involved irregularly by breast cancer.

The main goal of this research was to generate a procedure for enhancing the digital mammographic images, based on *wavelet transform methods*.

1.1 Brief Overview of the Discrete Wavelet Transformation (DWT)

Let $\mathbf{y}$ be a data-vector of dimension (size) n. For simplicity, we choose n to be a power of 2, say 2^J.

Suppose that we apply a wavelet transform to the vector $\mathbf{y}$ yielding a transformed vector $\mathbf{d}$ that has the same length as $\mathbf{y}$. This linear and orthogonal transform can be fully described by an $n \times n$ orthogonal matrix $\mathbf{W}$. In practice, one performs the DWT without exhibiting the matrix $\mathbf{W}$ explicitly, but by using fast filtering algorithms. The filtering procedures are based on so-called quadrature mirror filters which are uniquely determined by the wavelet of choice and fast Mallat's algorithm (Mallat [15]). The wavelet decomposition of the vector $\mathbf{y}$ can be written as

$$\mathbf{d} = (\mathcal{H}^{\ell}\mathbf{y}, \mathcal{G}\mathcal{H}^{\ell-1}\mathbf{y}, \ldots, \mathcal{G}\mathcal{H}^{2}\mathbf{y}, \mathcal{G}\mathcal{H}\mathbf{y}, \mathcal{G}\mathbf{y}). \tag{1}$$

where ℓ is any fixed number between 1 and $J = \log_2 n$, and the operators $\mathcal{H}$ and $\mathcal{G}$ are defined coordinate-wise by

$$(\mathcal{H}a)_k = \sum_{m \in \mathbf{Z}} h_{m-2k} a_m, \text{ and } (\mathcal{G}a)_k = \sum_{m \in \mathbf{Z}} g_{m-2k} a_m, \quad k \in \mathbf{Z}$$

where g and h are high- and low-pass filters corresponding to the wavelet of choice. Components of g and h are connected via the quadrature mirror relationship $g_n = (-1)^n h_{1-n}$. For all commonly used wavelet bases, the taps of filters g and h are readily available in the literature or in standard wavelet software packages.

The elements of $\mathbf{d}$ are called *wavelet coefficients*. The sub-vectors described in (1) correspond to detail levels in a levelwise organized decomposition. For

instance, the vector $\mathcal{G}\mathbf{y}$ contains $n/2$ coefficients representing the finest level of detail.

In general, jth detail level in the wavelet decomposition of $\mathbf{y}$ contains 2^j elements, and is given as

$$\mathcal{G}\mathcal{H}^{J-j-1}\mathbf{y} = (d_{j,0}, d_{j,1}, \ldots, d_{j,2^j-1}). \tag{2}$$

Wavelet transformations of 2-D objects (images) are performed by applying univariate transformations on the rows and on the columns of the 2-D object. One step of the decomposing algorithm is described next. Consider a digital image A, which is in fact a matrix comprised of pixel values. A wavelet decomposition begins by applying the wavelet low pass filter $\mathcal{H}$ and high pass filter $\mathcal{G}$ to the rows of the matrix A. This step produces two matrices $\mathcal{H}_r A$ and $\mathcal{G}_r A$, both of dimension $2^n \times 2^{n-1}$ (the subscripts r suggest that the filters are applied on rows). Next, the filters $\mathcal{H}$ and $\mathcal{G}$ are applied to the columns of the matrices $\mathcal{H}_r A$ and $\mathcal{G}_r A$ obtained from step one, producing matrices $\mathcal{H}_c\mathcal{H}_r A, \mathcal{G}_c\mathcal{H}_r A, \mathcal{H}_c\mathcal{G}_r A$ and $\mathcal{G}_c\mathcal{G}_r A$, each of dimension $2^{n-1} \times 2^{n-1}$. The matrix $\mathcal{H}_c\mathcal{H}_r A$ is an average or smooth representation of the original image, while the matrices $\mathcal{G}_c\mathcal{H}_r A, \mathcal{H}_c\mathcal{G}_r A$ and $\mathcal{G}_c\mathcal{G}_r A$ contain details lost by degrading A to $\mathcal{H}_c\mathcal{H}_r A$. The transform is further carried out by repeating the process on the *average* matrix $\mathcal{H}_c\mathcal{H}_r A$ in place of A. In the rest of the paper we denote $\mathcal{H}_c\mathcal{H}_r A$ simply by $\mathcal{H}\mathcal{H}$, $\mathcal{H}_c\mathcal{G}_r A$ by $\mathcal{H}\mathcal{G}$ and the other matrices correspondingly.

1.2 Previous work

Many computerized methods for detecting clustered microcalcifications based on wavelets have been proposed. Yoshida *et al.* [25] used a combined difference-image technique and a wavelet transform to detect subtle microcalcifications. First, the difference-image technique is used to increase the signal-to-noise ratio of microcalcifications, and then the wavelet-based scheme is applied to detect the subtle microcalcifications missed by the first step. To extract small-scale structures, wavelet transform (WT) uses a fine "probe" that is represented by a small wave.

Lado *et al.* [13] employed a computerized scheme for detecting "both individual microcalcifications in regions of interest (ROIs) and clustered microcalcifications over the complete mammograms, based on the application of two different wavelet transform techniques"(one-dimensional and two-dimensional WT). Wang *et al.* [24], proposed an approach for detecting microcalcifications in digital mammograms employing wavelet-based subband image decomposition is presented. In Anastasio *et al.* [2], the wavelet transform is employed as a preprocessing step whose goal is to enhance the microcalcifications and suppress the background structure in the mammogram. A parallel-genetic algorithm is used in performing the optimization of the CAD procedure.

Strickland *et al.* [21] developed a 2-stage method based on wavelet transforms for the detection and segmentation of calcifications. The first stage is based on an nondecimated wavelet transform.

In the second stage, detected pixel sites in $\mathcal{GG}$ and $\mathcal{HG} + \mathcal{GH}$ are dilated and then weighted before computing the inverse wavelet transform (here $\mathcal{GG}, \mathcal{HG}$ and $\mathcal{GH}$ denote the detail components in the second level of decomposition). Bruce and Adhami [3] apply the discrete wavelet transform mod-max method to the problem of mammographic mass classification. This method was used to extract multiresolution features that quantify the mass shapes. They showed that when utilizing a statistical classification system with Euclidian distance measures in determining class membership, the use of multiresolution features significantly increases the classification accuracy. Ferrari *et al.* [9] presented a method for the identification of pectoral muscle in MLO (mediolateral oblique) mammograms based on the multiresolution technique using Gabor wavelets. Chang *et al.* [4] developed an enhancement algorithm relying on multiscale wavelet analysis, and extracted oriented information at each scale of analysis was investigated. Another approach to image enhancement of digital mammography images was introduced by Seršić and Lončarić [19]. It consists of three steps: low-frequency tissue density component removal, noise filtering, and microcalcification enhancement. An overview of automatic methods for detection of microcalcifications was given in a recent publication by Thangavel *et al.* [22]. To our knowledge, none of the previous methods utilized the scaling property of the mammography images to obtain the subpixel enhancement.

2 Description of the data

The collection of images we analyzed was obtained from the University of South Florida's Digital Database for Screening Mammography (DDSM)(Heat *et al.* [10]). (See `http://marathon.csee.usf.edu/Mammography/Database.html`).
The DDSM is described in detail in Heat *et al.* [11]. Images containing suspicious areas have associated pixel-level "ground truth" information about the locations and types of suspicious regions. We selected a set of cases(studies) from the DDSM from volumes 6 and 7. Each case contains four mammograms (two for each breast, the craniocaudal (CC) and mediolateral oblique (MLO) projections) from a screening exam. We analyzed the data from 10 benign cases and 8 malignant cases, each containing calcifications.

The images were scanned on either a HOWTEK 960 or HOWTEK MultiRAD 850 digitizer with a sample rate of 43.5 microns per second at 12 bits per pixel. They were stored in a format using lossless JPEG compression. However, even with the compression, each image file is quite large because the films were scanned with resolution between 42 and 100 microns. The source code for the program used to compress, as well as the program used to uncompress the images are available to download from the web site.

3 Methodology

Wavelets have been applied for image enhancement since the early 1990's, and some of the prime applications are in digital mammography (Aldroubi and

Unser [1], Heinlein *et al.* [12], Lemaur *et al.* [14], McLeod *et al.* [16], Wang and Karayiannis [24], etc.) Most wavelet-based approaches involve thresholding, a procedure that eliminates background noise. Wavelets are also applied to generate "difference" images in which nonessential background is eliminated. The method proposed in this paper is novel and involves inverse wavelet transforms of low-resolution images. In what follows, we present a conceptual description of the WII procedure and demonstrate the utility of this approach for digital mammography.

Our approach consists of several steps. First, an image enhancement method is used to detect the *regions of interest* on each image. The area(s) with ROIs are then cropped from the original image. (From now on we will refer to those cropped images as the "original images.") To confirm that the correct regions were identified, we compared our ROIs with the information available from the DDSM where abnormalities were marked by experienced radiologists. After detecting the regions of interest on images from our data set, a three-level wavelet decomposition was applied to each image. In order to construct informative detail spaces, the WII procedure is combined with a *linear regression* approach, based on pixel intensity *scaling*, after which thresholding is applied on the resulting images. Finally, the 2-D inverse wavelet transform was applied using the original image as the smooth part and the estimated informative details to obtain a higher resolution enhanced image of microcalcifications.

We now describe each of these steps in more detail.

3.1 Detection of Regions of Interest (ROI)

We first consider an algorithm similar to that presented in Seršić and Lončarić [19], which aims to detect microcalcifications between $0.1mm$ and $1mm$ in diameter. Thus, in an original digital mammogram of $50\mu m \times 50\mu m$ resolution, a microcalcification may appear to be 2 to 20 pixels wide. A 5-level redundant 2D wavelet decomposition on the original mammogram yields detail coefficients with a spatial resolution from $0.1mm \times 0.1mm$ to $1.6mm \times 1.6mm$, thus encompassing the range of microcalcification size considered.

Wavelet coefficient images corresponding to the first level detail coefficients seem to consist primarily of spatially white noise, in the absence of microcalcifications between $0.05mm$ and $0.1mm$ in diameter. However, in the detail coefficients of levels $2-5$, the mammogram signal becomes apparent and microcalcifications begin to visually emerge from the background noise. The approximation coefficients at the 5^{th} level contain the low frequency mammogram information such as tissue density and breast shape information.

Several different wavelet families are considered for the ROI detection algorithm, but 2D polyharmonic B-spline wavelets with quincunx subsampling (see Van de Ville *et al.* [23]) are utilized due to their symmetry and lack of directional (horizontal, vertical, and diagonal) bias in the detection of microcalcifications. A significant difference between the algorithm presented here and that given in [19] is the use of a 2-D non-separable polyharmonic wavelet basis which introduces no directional bias due to the quincunx based subsampling scheme. The

algorithm presented by [19] utilizes recursive 1-D decompositions that favor horizontal, vertical, and diagonal directions, which may bias the structure of the microcalcifications.

3.2 Wavelet Image Interpolation procedure

The proposed WII procedure is conceptually simple. If the forward wavelet transform, described previously, degrades an image by decomposition into a smooth part and the details, then the inverse wavelet transform performed on a degraded image will interpolate the image and reveal a higher degree of details. Operationally, the procedure proceeds as follows:

1. One starts with an empty image (all entries 0) and performs k wavelet decomposition steps. Of course, the transform is linear and the resulting smooth and detail sub-matrices are all zero-matrices.
2. The degraded image from a digital mammogram is inserted into the position of the smooth matrix containing zeros. This step requires that the degraded input image and the original smooth part have equal dimensions. The detail matrices from step 1 retain the 0 values in all entries.
3. Back-transform the object by k steps.

This process increases the resolution of the degraded, pixelized image and contains 4^k times the number of pixels in the original input For example, a three-step transform produces an enhanced image with 64 times the number of pixels in the original degraded image. The main contribution of our algorithm is building detail spaces based on degraded image and general scaling properties of natural images.

3.3 Imputing Details

In the WII procedure described above, the three detail matrices, accompanying the pixelized image located in the smooth part, consist entirely of zero. It is natural to propose the utilization of detail spaces to further enhance the information in the interpolated image. Several avenues are possible, including template details, background details, wavelet-bootstrap by resampling the details, etc. Our proposal is to utilize the self-similarity of wavelet decompositions in building informative detail spaces.

Most of the natural images *scale* and this scaling can be assessed in the wavelet domain. Informally, scaling means that the "energy" (squared wavelet coefficients) cascades when the resolution of wavelet decomposition changes. This is particularly true for some medical images (tissue, bones, cancer, etc). This scaling was described and utilized in statistical inference by many researchers, see Aldrubi and Unser [1] and the references therein.

When an image possesses *regular scaling* this means that the logarithms of average energies in the detail spaces decay linearly when the resolution of scale increases. The standard 2-D wavelet transform has three detail components,

namely horizontal, vertical, and diagonal, and all are characterized by their intrinsic scaling.

In the standard multiresolution hierarchy of images, the representation space V_j is decomposed as

$$A_j = A_{j-1} + H_{j-1} + V_{j-1} + D_{j-1},$$

where the A_{j-1} is the coarser representation and $H_{j-1}, V_{j-1}, D_{j-1}$ are spaces of horizontal, vertical, and diagonal details. This representation is nested, and the coarse representation space A_{j-1} can be further split in the same fashion. Assume that the direction (horizontal, vertical or diagonal) of detail spaces is fixed. Suppose that $d_{j;k_1,k_2}$ is the wavelet coefficient at scale j at the location (k_1, k_2) and that E_j is the average of $d^2_{j;k_1,k_2}$ for all (k_1, k_2), i.e., $E_j = \frac{1}{N}\sum_{(k_1,k_2)} d^2_{j;k_1,k_2}$, where N is total number of coefficients at this particular detail space. By convention, j is a dyadic index corresponding to the base 2 logarithm of the scale. The scale decreases (resolution increases) with increasing indices j. Then,

$$\log E_j = \beta_0 + \beta_1 \times j, \tag{3}$$

with the slope β_1 characterizing regular scaling. The parameters β_0 and β_1 in (3) are estimated from the wavelet decomposition by the least-squares linear regression on pairs $(j, \log E_j)$ for a properly selected range of scale indices j, $j_0 \leq j \leq j_1$.

We utilize the intrinsic scaling in natural images to construct informative detail spaces. The algorithm is detailed below.

Algorithm description. The procedure begins with a three-level wavelet decomposition of the original coarse image. We denote the components of the first level decomposition by A_1, H_1, V_1, and D_1, and the components of level 2 and level 3 decomposition correspondingly.

Data sets were transformed to the wavelet domain utilizing the Daubechies 4 wavelet. To estimate the detail components, we then apply the following regression steps on the components (here illustrated only for horizontal detail components):

$$H_1^2 = \beta_0^{(1)} + \beta_1^{(1)} H_2^2\_\mathrm{e} \quad \text{and} \quad H_2^2 = \beta_0^{(2)} + \beta_1^{(2)} H_3^2\_\mathrm{e},$$

where the components are reshaped into vectors and H_2^2_e and H_3^2_e denote $H_2^{(2)}$ and $H_3^{(2)}$ vectors upsampled using the WII method. As we pointed out, the constant $\beta_1 < 0$ is connected to the global Hurst exponent; it describes intrinsic self-similarity of the image. The intercept β_0 depends on the total energy of the image and does not affect scaling. In our analysis, we actually found that the non-intercept model is appropriate.

Next, $\hat{H}_1$ and $\hat{H}_2$ are estimated as

$$\hat{H}_1 = [\hat{\beta}_0^{(1)} + \hat{\beta}_1^{(1)} H_2^2\_\mathrm{e}]^{1/2} \quad \text{and} \quad \hat{H}_2 = [\hat{\beta}_0^{(2)} + \hat{\beta}_1^{(2)} H_3^2\_\mathrm{e}]^{1/2}.$$

The sign of the generated detail coefficients is assigned to be the same as the sign in the observed coefficients in the degraded image. From the scaling property, the scaling coefficient k equals

$$k = \frac{\log E_{j-1} - \log E_j}{j - (j-1)} = \log \frac{E_{j-1}}{E_j}. \tag{4}$$

We then calculate the scaling coefficient k and use it to estimate the horizontal detail component H_0 as follows

$$k = \log\left(\frac{\bar{\hat{H}}_1^{\,2}}{\bar{\hat{H}}_{2\text{-e}}^{\,2}}\right) \Rightarrow k = \log\left(\frac{\bar{H}_0^2}{\bar{\hat{H}}_{1\text{-e}}^{\,2}}\right).$$

From this, we approximate H_0 as

$$H_0^2 = e^k \cdot \hat{H}_{1\text{-e}}^2 \quad \text{i.e.} \quad H_0 = [e^k \cdot \hat{H}_{1\text{-e}}^2]^{1/2}.$$

The generated object is "rich" in coefficients; to reduce dimension we apply the threshold, setting small detail coefficients to 0. We choose universal threshold (Donoho and Johnstone [7]) and note that other shrinkage strategies are possible.

The threshold $\lambda = \sqrt{2 \log N} \cdot \sigma$ is applied on the estimated wavelet coefficients. As an estimator of σ, we use the median absolute deviation (MAD) from the median:

$$\hat{\sigma} = \frac{1}{0.6745} \cdot \text{MAD}[d^{(f)}] = 1.4828 \cdot \text{median}[|\tilde{d}^{(f)} - \text{median}(\tilde{d}^{(f)}|],$$

where $\tilde{d}^{(f)}$ is the vector of finest detail coefficients associated to the multiresolution subspaces H, V, and D.

This procedure is repeated for the other two detail components (the vertical and the diagonal). Once we have the estimated detail components, we apply the inverse wavelet transform with our original coarse image as the smooth part and estimated detail components as details, to obtain a higher resolution enhanced image.

4 Results

The data analyzed in our study are from the University of South Florida's Digital Database for Screening Mammography (DDSM) [10]. (For more information see Section 2). We analyzed 8 malignant and 10 benign cases. Each case consists of four images, however in most cases microcalcifications were only found in one breast, hence we only analyzed the two corresponding images. In addition, some cases had multiple microcalcification sites, which resulted in 40 images we analyzed altogether. First, the ROI detection method described in Section 3.1 was applied to each of the images. ROIs were cropped to smaller images, which contained calcifications of approximately 0.05-1mm in dimension (in terms of

pixels: 20×20 to 50×50 pixels). Our main algorithm explained in 3.3 can be applied to $2^n \times 2^m$ pixels size images, it will here be illustrated on 64×64 images.

Figure 1 shows the result of applying the WII algorithm on an image of a malignant case. We notice a significant improvement from level 0 to level 1 and from level 1 to level 2, while there is only a very slight difference between levels 2 and 3. The images on Figure 1 were obtained by imputing zeros into the details

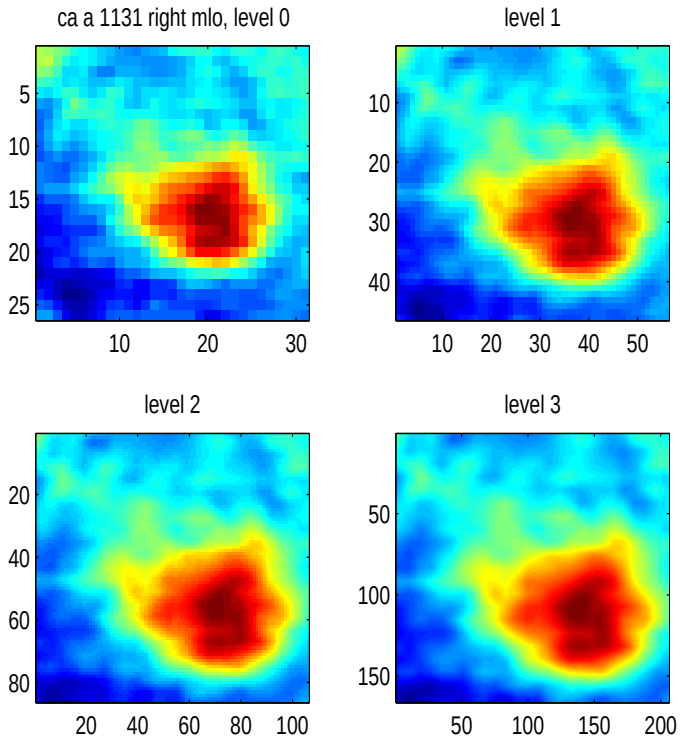

Fig. 1. Results of applying WII method on an image of a malignant calcification

components of the WII algorithm, with the original image as the smooth part.

Figure 2(left) shows another malignant case image (original image) with a cluster of microcalcifications. Figure 2(right) shows the result of our image enhancement algorithm, described in 3.3, applied on the image in Figure 2(left). We used the gray scale representations of the images since it follows the convention among the radiologists and was preferred by the clinical radiologist on our research team who made the clinical assessments of the images.

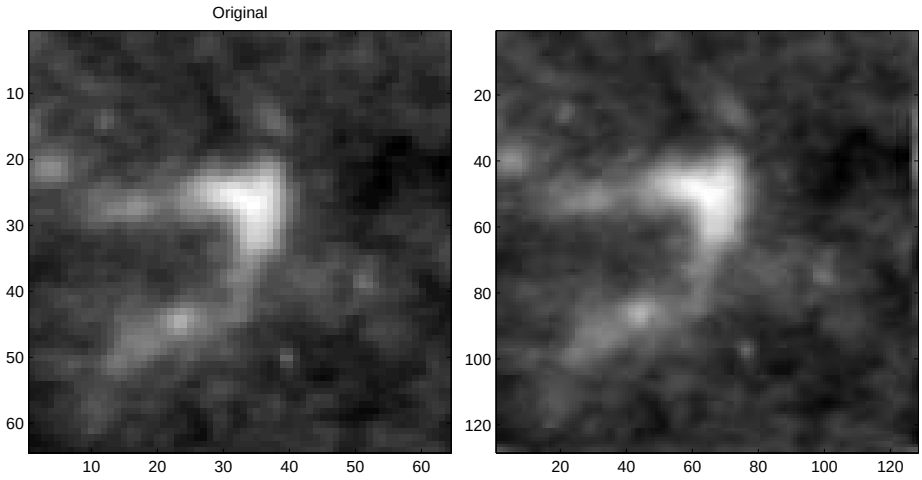

Fig. 2. Results of applying WII algorithm on an image of a malignant calcification(s); left: original image, right: enhanced image

Figure 3(left) shows an image of a benign case (original image). Figure 3(right) shows the result of the image enhancement algorithm, applied on the image in Figure 3(left).

5 Conclusions

Motivated by the ubiquitous presence of regular scaling in medical images, we propose a regression-based approach to extrapolate on the wavelet coefficients of an image to be enhanced. The observed image and its extrapolated details are then transformed by an inverse wavelet transform and the image of higher resolution is obtained. This process corresponds to a wavelet-based image interpolation that is improved by information about regular scaling in detail coefficients.

We found that our proposed procedure is efficient and useful in capturing relevant clinical information in the context of digital mammographic imaging. Our assessments were made by evaluations of the 18 knowns preformed by the clinical radiologist on our research team. We emphasize that at this point, the study is more of a feasibility type, than a stringent test of efficacy.

The improved visualization of calcium morphology is expected to translate to greater specificity in assigning degree of suspicion and need-for-biopsy for calcifications noted in mammography. More study with additional observers is planned to confirm what looks to be a novel helpful technology.

We envision several avenues for future algorithm enhancement. We plan to (i) develop new shrinkage strategies to explore alternatives to the traditional universal thresholding, (ii) to identify the wavelet that yields optimal performance for our application, and (iii) to formalize and to expand the evaluation phase with

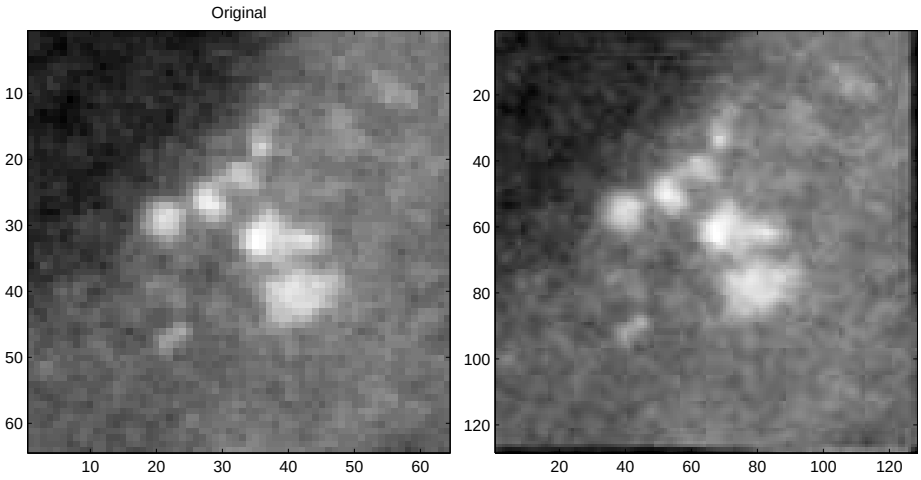

Fig. 3. Results of applying WII algorithm on an image of a benign calcification(s); left: original image, right: enhanced image

several radiologists involved in a blind repeated measures study design involving an extensive number of cases. We also plan to contrast the WII approach to other approaches based on quantitative or qualitative measures using the same images and the same team of observers.

References

1. Aldroubi, A. and Unser, M. A. (1996). *Wavelets in Medicine and Biology.*, CRC Press, Boca Raton FL, 616 p.
2. Anastasio, M., Yoshida, H., Nishikawa, R., Giger, M., and Dio, K. (1998). Global Optimization of Wavelet-Based Computer-Aided Diagnosis (CAD) Scheme for the Detection of Clustered Microcalcifications in Digital Mammograms", Kurt Rossmann Laboratories for Radiologic Image Research, Research Report.
3. Bruce, L. M. and Adhami, R. R. (1996). "Classifying Mammographic Mass Shapes Using the Wavelet Transform Modulus-Maxima Method", *IEEE Transactions on Medical Imaging*, pp. 1170–1177, 18 (12).
4. Chang, C-M. and Laine, A. (1996). Coherence of Multiscale Features for Enhancement of Digital Mammograms", *IEEE Transactions on Information Technology in Biomedicine*, 3, 32–46.
5. Coakley, K. and van Doorn T. (1995). Invariant moment shape description of microcalcifications in digital mammograms. *Australas Phys Eng Sci Med.* 18 (2), 114–118.
6. Curpen, B. N., Sickles, E. A., and Sollitto R. A. (1995). The comparative value of mammographic screening for women 40-49 years old versus women 50-59 years old. *AJR*, 164, 1099–1103.
7. Donoho, D. L. and Johnstone, I. M., "Ideal spatial adaptation via wavelet shrinkage", *Biometrika*, 91:425-455, 1994.

8. Egan, R., Sweeney, M., and Sewell, C. (1980). Intramammary calcifications without an associated mass in benign and malignant diseases, *Radiology.*
9. Ferrari, R. J. Rangayyan, R. M., Desautels, J. E. L., Borges, R. A. and Frere, A. F. (2004). Automatic Identification of the Pectoral Muscle in Mammograms", *IEEE TRansactions on Medical Imaging*, 23 (2), 232–245.
10. Heath, M., Bowyer, K.W., Kopans, D. *et al.* (1998). Current status of the Digital Database for Screening Mammography, *Digital Mammography*, pp 457–460, Kluwer Academic Publishers.
11. Heath, M., Bowyer, K., Kopans, D., Moore R., and Kegelmeyer P. Jr. (2000). The Digital Database for Screening Mammography, in *The Proceedings of the 5th International Workshop on Digital Mammography* (Toronto, Canada, June 2000), Medical Physics Publishing (Madison, WI), ISBN 1-930524-00-5.
12. Heinlein P., Drexl J., and Schneider W. (2003). Integrated wavelets for enhancement of microcalcifications in digital mammography. *IEEE Trans. Med. Imag.* 22 (3), 402–413.
13. Lado, M. J., Tahoces, P. G., Méndez, P. G., Souto, M. and Vidal, J. J. (1999). A Wavelet-based Algorithm for Detecting Clustered Microcalcifications in Digital Mammograms, *Med. Phys.*, 26 (7), 1294–1305.
14. Lemaur, K., Drouiche, J., and DeConinck, (2003). Highly Regular Wavelets for the Detection of Clustered Microcalcifications in Mammograms, *IEEE Trans. Med. Imag.*, 22(3), 393–401.
15. Mallat, S. (1989). A theory for multiresolution signal decomposition: The wavelet representation. *IEEE Trans. Pattern Anal. Machine Intell.*, 11, 674–693.
16. McLeod G., Parkin G. J. S., and Cowen A. R. (1996). Automatic detection of clustered micro-calcifications using Wavelets, In: , Eds. Doi K, pages 311–316, Publisher: Elsevier Science BV (Amsterdam).
17. Menges, V., Wellauer, J., Engeler, V., and Stadelmann, R. (1973). Correlation of numerically detected microcalcifications on the mammogram and in this manner diagnosed carcinomas and mastopathies, (in German), *Radiologe.* 13 (11), 468–476.
18. Millis, R., Davis, A., Stacey, M., Phil, M. (1976). The detection and significance of calcifications in the breast: A radiologic pathologic study, *Br. J. Radiol.*
19. Seršić, D. and Lončarić, S. (1998). Enhancement of Mammographic Images for Detection of Microcalcifications, *Proceedings of the IX European Signal Processing Conference*, Vol. 2, pp. 693-696, Island of Rhodos, Greece.
20. Smart, C. R., Hendrick, R. E., Rutledge J. H., and Smith, R. A. (1995). Benefit of mammography screening in women ages 40 to 49 years: current evidence from randomized controlled trials, *Cancer*,75, 1619–1626.
21. Strickland, R.N. and Hahn, H.I. (1996). Wavelet Transform for Detecting Microcalcifications in Mammograms, *IEEE Transactions on Medical Imaging*, Vol. 15, No.2, 218–229.
22. Thangavel, K., Karnan, M., Sivakumar, R. and Mohideen, A. K. (2005). Automatic Detection of Microcalcifications in Mammograms - A Review, *ICGST International Journal on Graphics, Vision and Image Processing, GVIP.*
23. Van de Ville D., Blu T., Unser M. (2007). Isotropic Polyharmonic B-splines: Scaling Functions and Wavelets, *IEEE Transactions on Image Processing*, In press.
24. Wang T. C. and Karayiannis N. B. (1998). Detection of microcalcifications in digital mammograms using wavelets, *IEEE Trans Med Imaging.* 17(4), 498–509.
25. Yoshida, H, Doi, K., Nishikawa, R. M., Ginger, M. L., and Schmidt, R. A. (1996). An Improved Computer-Assisted Scheme Using Wavelet Transform for Detecting Clustered Mirocalcifications in Digital images, *Acad Radiol*, 3, pp. 621–627.